The purpose of this chapter is to provide a brief introduction to the Standard Model of particle physics. In particular, it gives an overview of the fundamental particles and the relationship between these particles and the forces. It also provides an introduction to the interactions of particles in matter and how they are detected and identified in the experiments at modern particle colliders.

1.1 The Standard Model of particle physics

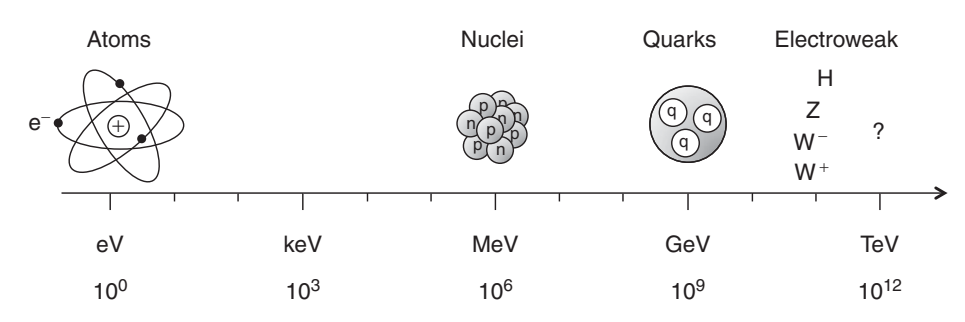
Particle physics is at the heart of our understanding of the laws of nature. It is concerned with the fundamental constituents of the Universe, the *elementary particles*, and the interactions between them, the *forces*. Our current understanding is embodied in the Standard Model of particle physics, which provides a unified picture where the forces between particles are themselves described by the exchange of particles. Remarkably, the Standard Model provides a successful description of all current experimental data and represents one of the triumphs of modern physics.

1.1.1 The fundamental particles

In general, physics aims to provide an effective mathematical description of a physical system, appropriate to the energy scale being considered. The world around us appears to be formed from just a few different particles. Atoms are the bound states of negatively charged electrons (e⁻) which orbit around a central nucleus composed of positively charged protons (p) and electrically neutral neutrons (n). The electrons are bound to the nucleus by the electrostatic attraction between opposite charges, which is the low-energy manifestation of the fundamental theory of electromagnetism, namely Quantum Electrodynamics (QED). The rich structure of the properties of the elements of the periodic table emerges from quantum mechanics, which dictates the precise electronic structure of the different atoms. In the atomic nucleus, the protons and neutrons are bound together by the strong nuclear force, which is a manifestation of the fundamental theory of strong interactions,

1

Fig. 1.1



The Universe at different energy scales, from atomic physics to modern particle physics at the TeV scale.

called Quantum Chromodynamics (QCD). The fundamental interactions of particle physics are completed by the weak force, which is responsible for the nuclear β-decays of certain radioactive isotopes and the nuclear fusion processes that fuel the Sun. In both nuclear β -decay and nuclear fusion, another particle, the nearly massless electron neutrino (ve) is produced. Almost all commonly encountered physical phenomena can be described in terms of the electron, electron neutrino, proton and neutron, interacting by the electromagnetic, strong and weak forces. The picture is completed by gravity, which although extremely weak, is always attractive and is therefore responsible for large-scale structure in the Universe. This is an appealingly simple physical model with just four "fundamental" particles and four fundamental forces. However, at higher energy scales, further structure is observed, as indicated in Figure 1.1. For example, the protons and neutrons are found to be bound states of (what are believed to be) genuinely fundamental particles called quarks, with the proton consisting of two up-quarks and a down-quark, p(uud), and the neutron consisting of two down-quarks and an up-quark, n(ddu).

The electron, the electron neutrino, the up-quark and down-quark are known collectively as the *first generation*. As far as we know, they are elementary particles, rather than being composite, and represent the basic building blocks of the low-energy Universe. However, when particle interactions are studied at the energy scales encountered in high-energy particle colliders, further complexity is revealed. For each of the four first-generation particles, there are exactly two copies which differ only in their masses. These additional eight particles are known as the *second* and *third generations*. For example, the muon (μ^-) is essentially a heavier version of the electron with mass $m_{\mu} \approx 200 \, m_{\rm e}$, and the third generation tau-lepton (τ^-) is an even heavier copy with $m_{\tau} \approx 3500 \, m_{\rm e}$. Apart from the differences in masses, which have physical consequences, the properties of the electron, muon and tau-lepton are the same in the sense that they possess exactly the same fundamental interactions.

It is natural to ask whether this pattern is repeated and that there are further generations of particles. Perhaps surprisingly, this seems not to be the case; there is

Table 1.1 The twelve fundamental fermions divided into quarks and leptons. The masses of the quarks are the current masses.								
	Leptons				Quarks			
	Partic	le	Q	mass/GeV	Partic	le	Q	mass/GeV
First	electron	(e ⁻)	-1	0.0005	down	(d)	-1/3	0.003
generation	neutrino	(ν_e)	0	$< 10^{-9}$	up	(u)	+2/3	0.005
Second	muon	(μ^-)	-1	0.106	strange	(s)	-1/3	0.1
generation	neutrino	(ν_{μ})	0	$< 10^{-9}$	charm	(c)	+2/3	1.3
Third	tau	(τ^{-})	-1	1.78	bottom	(b)	-1/3	4.5
generation	neutrino	(ν_τ)	0	< 10 ⁻⁹	top	(t)	+2/3	174

First generation	ν_{e}	e ⁻	d °	u °
Second generation	$ u_{\mu}$	μ-	s	c
Third generation	$\nu_{ au}$	τ	b	t

The particles in the three generations of fundamental fermions with the masses indicated by imagined spherical volumes of constant density. In reality, fundamental particles are believed to be point-like.

strong experimental evidence that there are just three generations; hence the matter content of the Universe appears to be in the form of the twelve fundamental spinhalf particles listed in Table 1.1. There is a subtlety when it comes to the description of the neutrinos; the $\nu_e,\,\nu_\mu$ and ν_τ are in fact quantum-mechanical mixtures of the three fundamental neutrino states with well-defined masses, labelled simply $\nu_1,\,\nu_2$ and ν_3 . This distinction is only important in the discussion of the behaviour of neutrinos that propagate over large distances, as described in Chapter 13. Whilst it is known that the neutrinos are not massless, the masses are sufficiently small that they have yet to be determined. From the upper limits on the possible neutrino masses, it is clear that they are at least nine orders of magnitude lighter than the other fermions. Apart from the neutrinos, the masses of the particles within a particular generation are found to be rather similar, as illustrated in Figure 1.2. Whilst it is likely that there is some underlying reason for this pattern of masses, it is not currently understood.

Fig. 1.2

Table 1.2 The forces experienced by different particles.							
					strong	electromagnetic	weak
Quarks	down-type up-type	d u	s c	b	√	✓	✓
Leptons	charged	e ⁻	μ-	τ-		✓	√
•	neutrinos	$v_{\rm e}$	$ u_{\mu}$	$ u_{ au}$			√

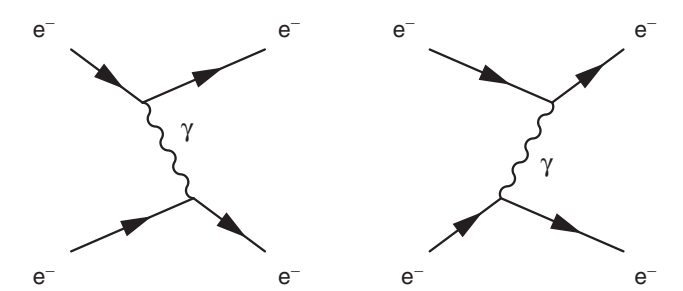
The dynamics of each of the twelve fundamental fermions are described by the Dirac equation of relativistic quantum mechanics, which is the subject of Chapter 4. One important consequence of the Dirac equation is that for each of the twelve fermions there exists an antiparticle state with exactly the same mass, but opposite charge. Antiparticles are denoted either by their charge or by a bar over the corresponding particle symbol. For example, the anti-electron (which is known as the positron) is denoted by e^+ , and the anti-up-quark is written \overline{u} .

Quarks and leptons

The particles interact with each other through the four fundamental forces, gravity, electromagnetism, the strong force and the weak force. The gravitational force between two individual particles is extremely small and can be neglected in the discussion of particle interactions. The properties of the twelve fundamental fermions are categorised by the types of interaction that they experience, as summarised in Table 1.2. All twelve fundamental particles "feel" the weak force and undergo weak interactions. With the exception of the neutrinos, which are electrically neutral, the other nine particles are electrically charged and participate in the electromagnetic interaction of QED. Only the quarks carry the QCD equivalent of electric charge, called *colour charge*. Consequently, only the quarks feel the strong force. Because of the nature of the QCD interaction, quarks are never observed as free particles, but are always confined to bound states called *hadrons*, such as the proton and neutron. Because the quarks feel the strong force, their properties are very different from those of the electron, muon, tau-lepton and the neutrinos, which are collectively referred to as the *leptons*.

1.1.2 The fundamental forces

In classical electromagnetism, the electrostatic force between charged particles can be described in terms of a scalar potential. This classical description of a force arising from a potential is unsatisfactory on a number of levels. For example, when an electron scatters in the electrostatic potential of a proton, there is a transfer of momentum from one particle to the other without any apparent mediating body.



The scattering of two electrons in QED by the exchange of a photon. With time running from left to right, the diagrams indicate the two possible time-orderings.

Regarding this apparent action-at-a-distance, Newton famously wrote "It is inconceivable that inanimate brute matter should, without the mediation of something else which is not material, operate upon and affect other matter without mutual contact". Whilst it is convenient to express classical electromagnetism in terms of potentials, it hides the fundamental origin of the electromagnetic interaction.

In modern particle physics, each force is described by a Quantum Field Theory (QFT). In the case of electromagnetism this is the theory of Quantum Electrodynamics (QED), where the interactions between charged particles are mediated by the exchange of *virtual* photons; the meaning of the term virtual is explained in Chapter 5. By describing a force in terms of particle exchange, there is no longer any mysterious action at a distance. As an example, Figure 1.3 shows the interaction between two electrons by the exchange of a photon. In the first diagram, the upper electron emits a photon, which at a later time is absorbed by the lower electron. The effect is to transfer momentum from one electron to the other, and it is this transfer of momentum which manifests itself as a force. The second diagram shows the other possible time-ordering with the lower electron emitting the photon that is subsequently absorbed by the upper electron. Since the exchanged particle is not observed, only the combined effect of these two time-ordered diagrams is physically meaningful.

Each of the three forces of relevance to particle physics is described by a QFT corresponding to the exchange of a spin-1 force-carrying particle, known as a gauge boson. The familiar spin-1 photon is the gauge boson of QED. In the case of the strong interaction, the force-carrying particle is called the gluon which, like the photon, is massless. The weak charged-current interaction, which is responsible for nuclear β -decay and nuclear fusion, is mediated by the charged W^+ and W^- bosons, which are approximately eighty times more massive than the proton. There is also a weak neutral-current interaction, closely related to the charged current, which is mediated by the electrically neutral Z boson. The relative strengths of the forces associated with the different gauge bosons are indicated in Table 1.3. It should be noted that these numbers are only indicative as the strengths of the forces depend on the distance and energy scale being considered.

The four known forces of nature. The relative strengths are approximate indicative values for two
fundamental particles at a distance of 1 fm = 10^{-15} m (roughly the radius of a proton).

Force	Strength	Boson		Spin	Mass/GeV
Strong	1	Gluon	g	1	0
Electromagnetism	10^{-3}	Photon	γ	1	0
Weak	10^{-8}	W boson	W^{\pm}	1	80.4
weak	10 °	Z boson	Z	1	91.2
Gravity	10^{-37}	Graviton?	G	2	0

1.1.3 The Higgs boson

The final element of the Standard Model is the Higgs boson, which was discovered by the ATLAS and CMS experiments at the Large Hadron Collider (LHC) in 2012. The Higgs boson, which has a mass

$$m_{\rm H} \approx 125\,{\rm GeV}$$
,

differs from all other Standard Model particles. Unlike, the fundamental fermions and the gauge bosons, which are respectively spin-half and spin-1 particles, the Higgs boson is spin-0 scalar particle. As conceived in the Standard Model, the Higgs boson is the only fundamental scalar discovered to date.

The Higgs boson plays a special rôle in the Standard Model; it provides the mechanism by which all other particles acquire mass. Without it the Universe would be a very different, all the particles would be massless and would propagate at the speed of light! In QFT, the Higgs boson can be thought of as an excitation of the Higgs field. Unlike the fields associated with the fundamental fermions and bosons, which have zero expectation values in the vacuum, the Higgs field is believed to have a non-zero vacuum expectation value. It is the interaction of the initially massless particles with this non-zero Higgs field that gives them their masses. The discovery of a Higgs-like particle at the LHC represented a remarkable validation of the theoretical ideas which constitute the Standard Model. The mathematical details of the Higgs mechanism, which are subtle, are discussed in detail in Chapter 17. The masses of the W[±], Z and H bosons are all of the order of 100 GeV, which is known as the electroweak scale. This doesn't happen by chance; in the Standard Model, the masses of the weak gauge bosons are intimately connected to the Higgs mechanism.

1.1.4 The Standard Model vertices

The nature of the strong, electromagnetic and weak forces are determined by the properties of the bosons of the associated quantum field theory, and the way in

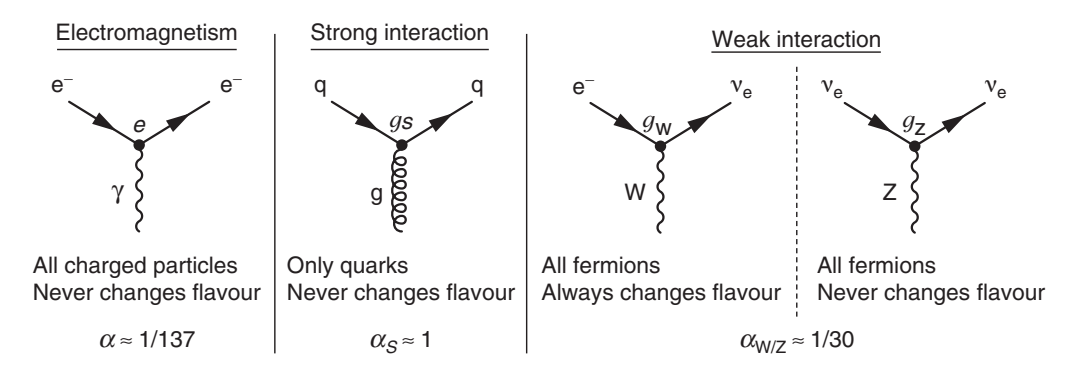


Fig. 1.4 The Standard Model interaction vertices.

which the gauge bosons couple to the spin-half fermions. The coupling of the gauge bosons to the fermions is described by the Standard Model interaction vertices, shown in Figure 1.4. In each case, the interaction is a three-point vertex of the gauge boson and an incoming and outgoing fermion. For each type of interaction there is an associated coupling strength g. For QED the coupling strength is simply the electron charge, $g_{\text{QED}} = e \equiv +|e|$.

A particle couples to a force-carrying boson only if it carries the charge of the interaction. For example, only electrically charged particles couple to the photon. Only the quarks carry the colour charge of QCD, and hence only quarks participate in the strong interaction. All twelve fundamental fermions carry the charge of the weak interaction, known as weak isospin, and therefore they all participate in the weak interaction. The weak charged-current interaction does not correspond to the usual concept of a force as it couples together different flavour fermions. Since the W^+ and W^- bosons have charges of +e and -e respectively, in order to conserve electric charge, the weak charged-current interaction only couples together pairs of fundamental fermions that differ by one unit of electric charge. In the case of the leptons, by definition, the weak interaction couples a charged lepton with its corresponding neutrino,

$$\left(\begin{array}{c} \nu_e \\ e^- \end{array}\right), \left(\begin{array}{c} \nu_\mu \\ \mu^- \end{array}\right), \left(\begin{array}{c} \nu_\tau \\ \tau^- \end{array}\right).$$

For the quarks, the weak interaction couples together all possible combinations differing by one unit of charge,

$$\begin{pmatrix} u \\ d \end{pmatrix}, \begin{pmatrix} u \\ s \end{pmatrix}, \begin{pmatrix} u \\ b \end{pmatrix}, \begin{pmatrix} c \\ d \end{pmatrix}, \begin{pmatrix} c \\ s \end{pmatrix}, \begin{pmatrix} c \\ b \end{pmatrix}, \begin{pmatrix} t \\ d \end{pmatrix}, \begin{pmatrix} t \\ s \end{pmatrix}, \begin{pmatrix} t \\ b \end{pmatrix}.$$

The strength of the weak charged-current coupling between the charge $+\frac{2}{3}$ uptype quarks (u, c, t) and the charge $-\frac{1}{3}$ down-type quarks (d, s, b) is greatest for quarks of the same generation. Since the weak interaction is the only known force

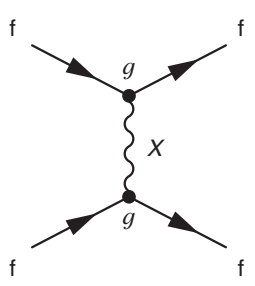


Fig. 1.5 The scattering of two fermions, denoted f, by the exchange of the boson, X. The strength of the fundamental interaction at each of the two three-point ffX vertices is denoted by the coupling constant g.

for which the incoming and outgoing fermions are different, the weak chargedcurrent interaction is particularly important when considering particle decays as it introduces a change of flavour.

The strength of the fundamental interaction between the gauge boson and a fermion is determined by the coupling constant g, which can be thought of as a measure of the probability of a spin-half fermion emitting or absorbing the boson of the interaction. Put more precisely, the quantum-mechanical transition matrix element for an interaction process includes a factor of the coupling constant g for each interaction vertex. For example, the matrix element for the scattering process indicated by Figure 1.5 contains two factors of g, one at each vertex, and therefore

$$\mathcal{M} \propto q^2$$
.

Hence, the interaction probability, which is proportional to the matrix element squared, $|\mathcal{M}|^2 = \mathcal{M}\mathcal{M}^*$, contains a factor g^2 from *each* interaction vertex, thus in this example

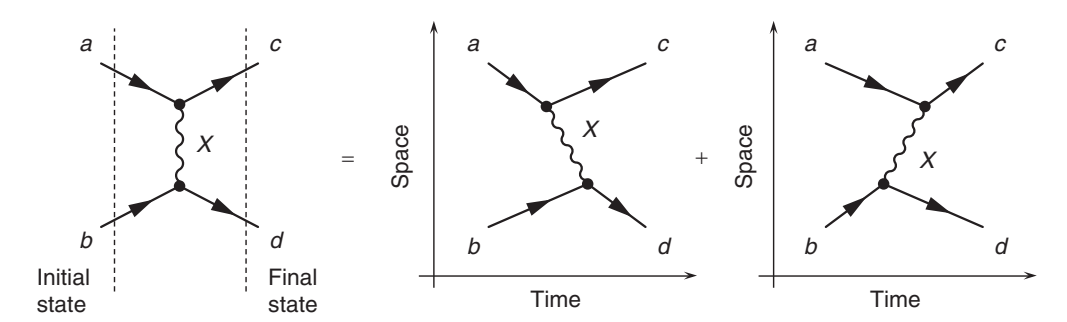
$$|\mathcal{M}|^2 \propto q^4$$
.

Rather than working with the coupling constant itself, it is often more convenient to use the associated dimensionless constant, $\alpha \propto g^2$. In the case of electromagnetism this is the familiar fine-structure constant

$$\alpha = \frac{e^2}{4\pi\varepsilon_0\hbar c}.$$

One advantage of writing the coupling strength in terms of a dimensionless constant is that the numerical value is independent of the system of units used for a calculation. In addition, the quantum-mechanical probability of the interaction includes a single factor of α for each interaction vertex. The intrinsic strength of the electromagnetic interaction is given by the size of fine-structure constant $\alpha = 1/137$. The QCD interaction is intrinsically stronger with $\alpha_S \sim 1$. The *intrinsic* strength of the weak interaction, with $\alpha_W \sim 1/30$, is in fact greater than that

Fig. 1.6



The Feynman diagram for the scattering process $a+b\to c+d$ and the two time-ordered processes that it represents.

of QED. However, the large mass of the associated W boson means that at relatively low-energy scales, such as those encountered in particle decays, the weak interaction is (as its name suggests) very much weaker than QED.

1.1.5 Feynman diagrams

Feynman diagrams are an essential part of the language of particle physics. They are a powerful representation of transitions between states in quantum field theory and represent all possible time-orderings in which a process can occur. For example, the generic Feynman diagram for the process $a + b \rightarrow c + d$, involving the exchange of boson X, shown in Figure 1.6, represents the sum of the quantum mechanical amplitudes for the two possible time-orderings. It should be remembered that in a Feynman diagram time runs from left to right but only in the sense that the left-hand side of a Feynman diagram represents the initial state, in this case particles a and b, and the right-hand side represents the final state, here c and d. The central part of the Feynman diagram shows the particles exchanged and the Standard Model vertices involved in the interaction, but not the order in which these processes occurred. Feynman diagrams are much more than a pictorial representation of the fundamental physics underlying a particular process. From Quantum Field Theory it is possible to derive simple Feynman rules associated with the vertices and virtual particles in a Feynman diagram. Once the Feynman diagram has been drawn, it is straightforward to write down the quantum-mechanical transition matrix element using the relevant Feynman rules, thus avoiding the need to calculate each process from first principles in Quantum Field Theory.

In general, for each process considered, there will be an infinite number of Feynman diagrams that can be drawn. For example, Figure 1.7 shows Feynman diagrams for the scattering of two electrons by the exchange of either one or two photons. Both diagrams have the same initial and final state, and therefore correspond to the same physical process, $e^-e^- \rightarrow e^-e^-$. Each interaction vertex is associated with a factor e in the matrix element, or equivalently a factor of α in the matrix

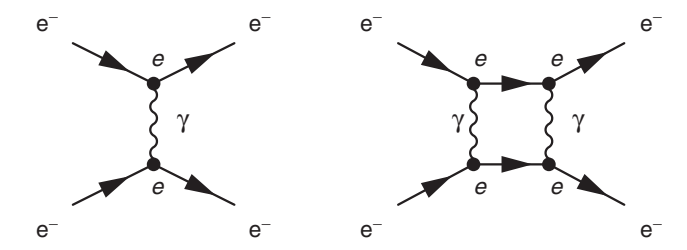


Fig. 1.7 Two Feynman diagrams for $e^-e^- \rightarrow e^-e^-$ scattering.

element squared. Thus, the matrix element squared for the diagram involving a single photon exchange and two vertices is proportional to α^2 , and that involving two photons and four vertices is proportional to α^4 ,

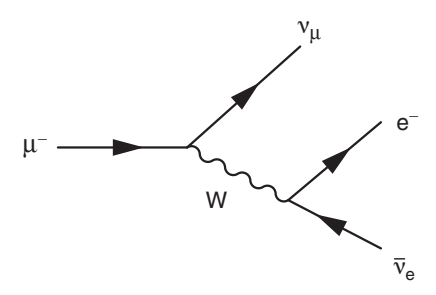
$$|\mathcal{M}_{\gamma}^2| \propto \alpha^2$$
 and $|\mathcal{M}_{\gamma\gamma}^2| \propto \alpha^4$.

Because the coupling strength of the electromagnetic interaction is relatively small, $\alpha \sim 1/137$, the diagram with four vertices is suppressed by a factor $O(10^4)$ relative to the diagram with two vertices. In the language of perturbation theory, only the lowest-order term is significant. Consequently, for almost all processes that will be encountered in this book, only the simplest (i.e. lowest-order) Feynman diagram needs to be considered.

For reasons that will become clear in Chapter 4, antiparticles are drawn in Feynman diagrams with arrows pointing in the "backwards in time" direction. In the Standard Model, particles and antiparticles can be created or annihilated only in pairs. This means that the arrows on the incoming and outgoing fermion lines in Standard Model vertices are always in the same sense and flow through the vertex; they never both point towards or away from the vertex.

1.1.6 Particle decays

Most particles decay with a very short lifetime. Consequently, only the relatively few stable and long-lived types of particle are detected in particle physics experiments. There are twelve fundamental spin-half particles (and the twelve corresponding antiparticles), but they are not all stable. For a particle to decay there must be a final state with lower total rest mass that can be reached by a process with a Feynman diagram constructed from the Standard Model vertices. Decays of the fundamental particles all involve the weak charged current which has the only interaction vertex that allows for a change in flavour. For example, since $m_{\mu} > m_{e}$ and the neutrinos are almost massless, the muon can decay via $\mu^{-} \rightarrow e^{-} \overline{\nu}_{e} \nu_{\mu}$ through the weak charged-current process with the Feynman diagram of Figure 1.8. Similar diagrams can be drawn for the tau-lepton. Since the electron is the lightest charged lepton, there is no corresponding weak decay process which conserves energy and momentum and consequently the electron is stable.



ig. 1.8 The Feynman diagram for muon decay. The arrow in the "negative time direction" denotes an antiparticle, in this case an electron antineutrino $(\overline{\nu}_e)$.

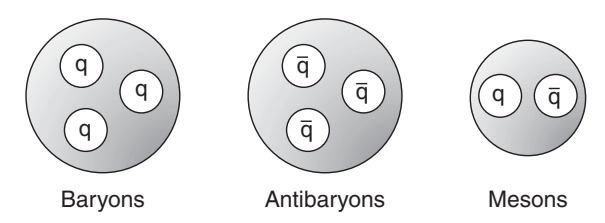


Fig. 1.9 The three types of observed hadronic states.

Because of the nature of the QCD interaction, quarks are never observed as free particles but are always found confined in bound states, known as hadrons. Consequently their decays need to be considered in the context of these bound states. The only hadronic states that have been observed to date, indicated in Figure 1.9, are the *mesons* which consist of a quark and an antiquark $(q\bar{q})$, the *baryons* which consist of three quarks (qqq), and the *antibaryons* consisting of three antiquarks $(q\bar{q})$.

Many hadronic states have been observed. These correspond to different combinations of quark flavours and different internal angular momenta states. Each of these distinct states is observed as a particle with a particular mass, which is not just the sum of the masses of the constituent quarks, but includes a large contribution from the QCD binding energy. The total angular momentum of a hadron, which is referred to as its spin, depends on the orbital angular momentum between the constituent quarks and the overall spin state. Hadronic states can be labelled by their flavour content, i.e. the type of quarks they contain, their total angular momentum J, and their parity P, which is an observable quantum number reflecting the symmetry of the wavefunction under the transformation $\mathbf{r} \to -\mathbf{r}$. For example, the positively charged pion $\pi^+(u\bar{d})$, which is the lightest meson state consisting of an up-quark and an anti-down-quark, has spin-parity $J^P = 0^-$. The masses and lifetimes for a number of commonly encountered hadrons are given in Appendix C.

The only stable hadron is the proton, which is the lightest system of three quarks with $m_p = 938.3 \text{ MeV} \equiv 1.673 \times 10^{-27} \text{ kg}$. As a free particle, the neutron with mass $m_n = 939.6 \text{ MeV}$, decays with a lifetime of about 15 min via the weak interaction

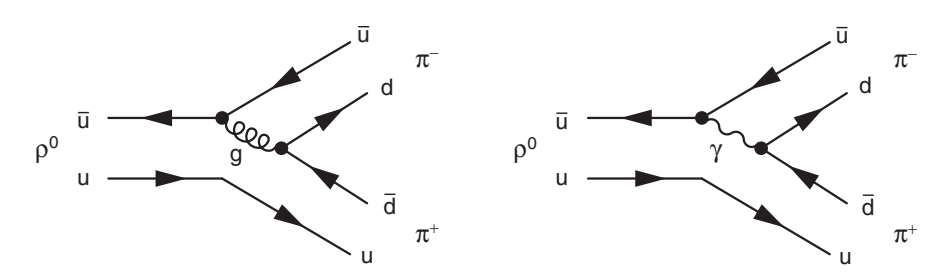


Fig. 1.10 Two possible Feynman diagrams for the decay $ho^0 o \pi^+\pi^-$.

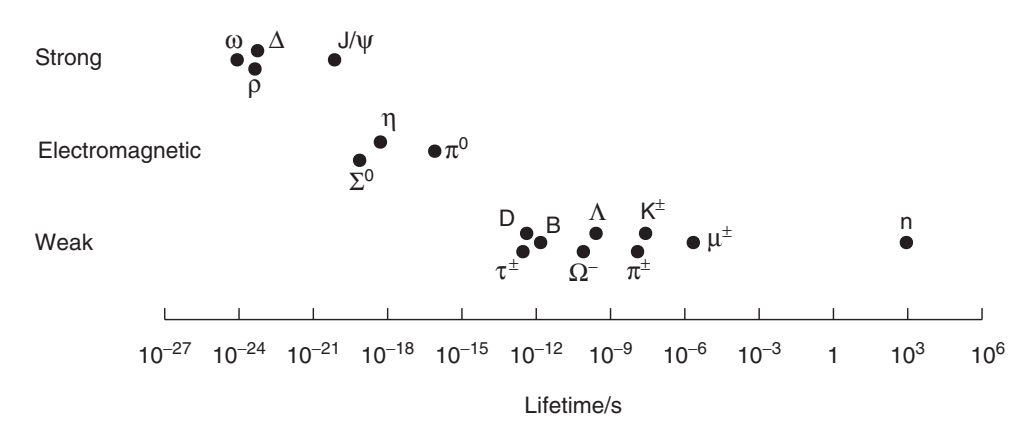


Fig. 1.11 The lifetimes of a number of common hadronic states grouped into the type of decay. Also shown are the lifetimes of the muon and tau-lepton, both of which decay weakly.

process $n \to p \, e^- \, \overline{\nu}_e$. Although a free neutron can decay, when bound within a nucleus, the change in nuclear binding energy is usually larger than the protonneutron mass difference, and under these circumstances the neutron behaves as a stable particle. All other hadronic states decay, usually very rapidly.

Whilst particle decay rates depend on a number of factors, the most important is the type of fundamental interaction involved in the decay. For example, Figure 1.10 shows two possible Feynman diagrams for the decay of the ρ^0 meson, $\rho^0 \to \pi^+\pi^-$. The first diagram is a strong decay involving the exchange of a gluon. The second diagram is an electromagnetic process. The respective matrix elements depend on the coupling strengths of the strong and electromagnetic forces,

$$|\mathcal{M}_{\rm g}|^2 \propto \alpha_{\rm S}^2$$
 and $|\mathcal{M}_{\gamma}|^2 \propto \alpha^2$.

Because α_S is two orders of magnitude greater than α , the contribution from the strong decay Feynman diagram dominates.

The above example illustrates an important point; if a particle can decay by the strong interaction this will almost always dominate over any possible electromagnetic or weak decay processes. Similarly, electromagnetic decay modes will dominate over weak interaction processes. To illustrate this point, Figure 1.11 shows the lifetimes of a selection of hadrons divided according to whether the dominant

decay mode is a strong, electromagnetic or weak interaction. Particles where only weak decay processes are possible are relatively long-lived (at least in the context of particle physics). Nevertheless, because the charged-current weak interaction produces a change of flavour at the interaction vertex, the weak interaction plays an important role in the decays of many particles for which electromagnetic and strong decay modes are not possible. Because many particles have very short lifetimes, only their decay products are observed in particle physics experiments.

1.2 Interactions of particles with matter

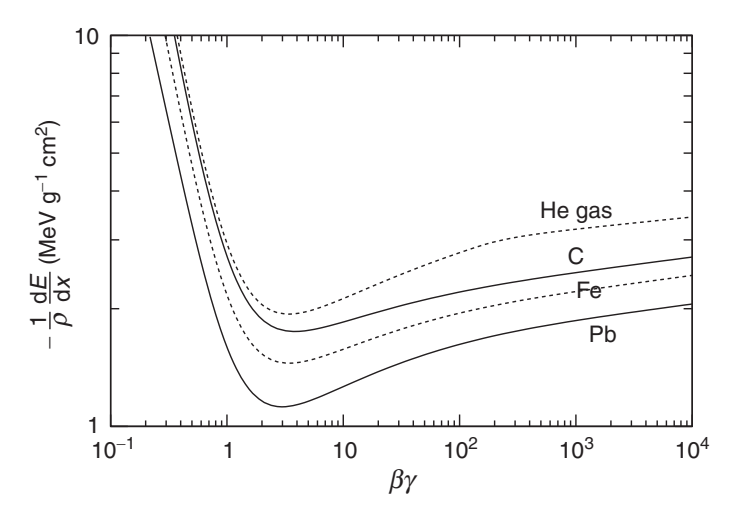
Particle physics experiments are designed to detect and identify the particles produced in high-energy collisions. Of the particles that can be produced, only the electron, proton, photon and the effectively undetectable neutrinos are stable. Unstable particles will travel a distance of order $\gamma v \tau$ before decaying, where τ is the mean lifetime (in the rest frame of the particle) and $\gamma = 1/\sqrt{1-v^2/c^2}$ is the Lorentz factor accounting for relativistic time dilation. Relativistic particles with lifetimes greater than approximately $10^{-10}\,\mathrm{s}$ will propagate over several metres when produced in high-energy particle collisions and thus can be directly detected. These relatively long-lived particles include the muon μ^\pm , the neutron n(ddu), the charged pions $\pi^+(u\bar{d})/\pi^-(d\bar{u})$, and the charged kaons $K^+(u\bar{s})/K^-(s\bar{u})$. Short-lived particles with lifetimes of less than $10^{-10}\,\mathrm{s}$ will typically decay before they travel a significant distance from the point of production and only their decay products can be detected.

The stable and relatively long-lived particles form the observables of particle physics collider experiments. The techniques employed to detect and identify the different particles depends on the nature of their interactions in matter. Broadly speaking, particle interactions can be divided into three categories: (i) the interactions of charged particles; (ii) the electromagnetic interactions of electrons and photons; and (iii) the strong interactions of charged and neutral hadrons.

1.2.1 Interactions and detection of charged particles

When a relativistic charged particle passes through a medium, it interacts electromagnetically with the atomic electrons and loses energy through the ionisation of the atoms. For a singly charged particle with velocity $v = \beta c$ traversing a medium with atomic number Z and number density n, the ionisation energy loss per unit length traversed is given by the Bethe–Bloch equation,

$$\frac{\mathrm{d}E}{\mathrm{d}x} \approx -4\pi\hbar^2 c^2 \alpha^2 \frac{nZ}{m_{\rm e} \mathrm{v}^2} \left\{ \ln \left[\frac{2\beta^2 \gamma^2 c^2 m_{\rm e}}{I_{\rm e}} \right] - \beta^2 \right\}. \tag{1.1}$$



The ionisation energy loss curves for a singly charged particle traversing lead, iron, carbon and gaseous helium. Adapted from Beringer *et al.* (2012).

Here I_e is the effective ionisation potential of the material averaged over all atomic electrons, which is very approximately given by $I_e \sim 10 \, Z \, \text{eV}$. For a particular medium, the rate of the ionisation energy loss of a charged particle is a function of its velocity. Owing to the $1/v^2$ term in the Bethe–Bloch equation, dE/dx is greatest for low-velocity particles. Modern particle physics is mostly concerned with highly relativistic particles where $v \approx c$. In this case, for a given medium, dE/dx depends logarithmically on $(\beta \gamma)^2$, where

$$\beta \gamma = \frac{v/c}{\sqrt{1 - (v/c)^2}} = \frac{p}{mc},$$

resulting in a slow "relativistic rise" of the rate of ionisation energy loss that is evident in Figure 1.12.

The rate of ionisation energy loss does not depend significantly on the material except through its density ρ . This can be seen by expressing the number density of atoms as $n = \rho/(Am_u)$, where A is the atomic mass number and $m_u = 1.66 \times 10^{-27}$ kg is the unified atomic mass unit. Hence (1.1) can be written

$$\frac{1}{\rho} \frac{\mathrm{d}E}{\mathrm{d}x} \approx -\frac{4\pi\hbar^2 c^2 \alpha^2}{m_{\rm e} v^2 m_u} \frac{Z}{A} \left\{ \ln \left[\frac{2\beta^2 \gamma^2 m_{\rm e} c^2}{I_{\rm e}} \right] - \beta^2 \right\},\tag{1.2}$$

and it can be seen that dE/dx is proportional to Z/A. Because nuclei consist of approximately equal numbers of protons and neutrons, Z/A is roughly constant and thus the rate of energy loss by ionisation is proportional to density but otherwise does not depend strongly on the material. This can be seen from Figure 1.12, which shows the ionisation energy loss (in units of MeV g^{-1} cm²) as a function of $\beta\gamma$ for a singly charged particle in helium, carbon, iron and lead. Particles with $\beta\gamma \approx 3$,

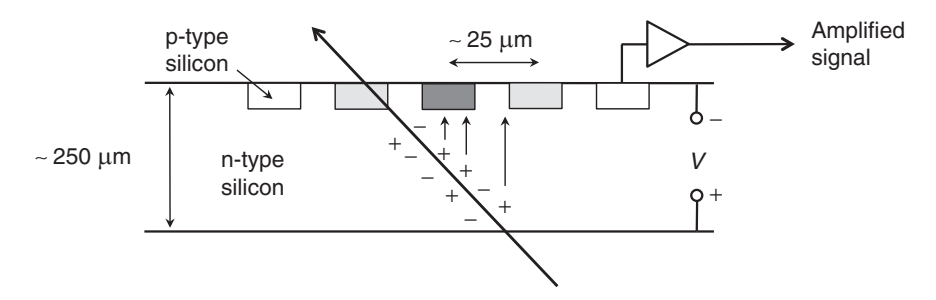
which corresponds to the minimum in the ionisation energy loss curve, are referred to as minimum ionising particles.

All charged particles lose energy through the ionisation of the medium in which they are propagating. Depending on the particle type, other energy-loss mechanisms maybe present. Nevertheless, for muons with energies below about 100 GeV, ionisation is the dominant energy-loss process. As a result, muons travel significant distances even in dense materials such as iron. For example, a 10 GeV muon loses approximately 13 MeV cm⁻¹ in iron and therefore has a range of several metres. Consequently, the muons produced at particle accelerators are highly penetrating particles that usually traverse the entire detector, leaving a trail of ionisation. This feature can be exploited to identify muons; all other charged particles have other types of interactions in addition to ionisation energy loss.

Tracking detectors

The detection and measurement of the momenta of charged particles is an essential aspect of any large particle physics experiment. Regardless of the medium through which a charged particle travels, it leaves a trail of ionised atoms and liberated electrons. By detecting this ionisation it is possible to reconstruct the trajectory of a charged particle. Two main tracking detector technologies are used. Charged particle tracks can detected in a large gaseous tracking volume by drifting the liberating electrons in a strong electric field towards sense wires where a signal can be recorded. However, in recent particle physics experiments, for example the ATLAS and CMS experiments at the LHC, there has been a move to using tracking detectors based on semiconductor technology using silicon pixels or strips.

When a charged particle traverses an appropriately doped silicon wafer, electronhole pairs are created by the ionisation process, as indicated by Figure 1.13. If a potential difference is applied across the silicon, the holes will drift in the direction of the electric field where they can be collected by p-n junctions. The sensors can be shaped into silicon strips, typically separated by $O(25 \,\mu\text{m})$, or into silicon pixels giving a precise 2D space point. The signals are not small; in crossing a typical silicon wafer, a charged particle will liberate $O(10\,000)$ electron-hole pairs that,



The production and collection of charge in a silicon tracking sensor.

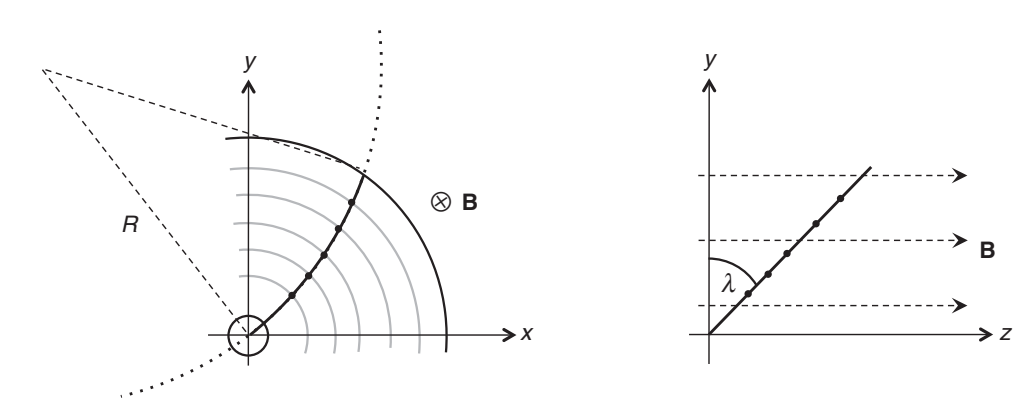


Fig. 1.14 The principle of charged particle track reconstruction from the space points observed in a (five-layer) silicon tracking detector. The curvature in the *xy*-plane determines the transverse momentum.

with appropriate amplification electronics, gives a clear signal associated with the strip/pixel on which the charge was collected.

Silicon tracking detectors typically consist of several cylindrical surfaces of silicon wafers, as indicated in Figure 1.14. A charged particle will leave a "hit" in a silicon sensor in each cylindrical layer from which the trajectory of the charged particle *track* can be reconstructed. The tracking system is usually placed in a large solenoid producing an approximately uniform magnetic field in the direction of axis of the colliding beams, taken to be the *z*-axis. Owing to the $\mathbf{v} \times \mathbf{B}$ Lorentz force, the trajectory of a charged particle in the axial magnetic field is a helix with a radius of curvature R and a pitch angle λ , which for a singly charged particle (|q| = e) are related to its momentum by

$$p\cos\lambda = 0.3 BR$$
,

where the momentum p is given in GeV/c, B is the magnetic flux density in tesla and R is in metres. Hence by determining the parameters of the helical trajectory from the measured hits in the tracking detectors, R and λ can be obtained and thus the momentum of the particle can be reconstructed. For high-momentum particles, the radius of curvature can be large. For example, the radius of curvature of a $100\,\text{GeV}$ π^\pm in the $4\,\text{T}$ magnetic field of the super-conductor solenoid of the CMS experiment is $R\sim 100\,\text{m}$. Even though such charged particle tracks appear almost straight, the small deflection is easily measured using the precise space-points from the silicon strip detectors.

Scintillation detectors

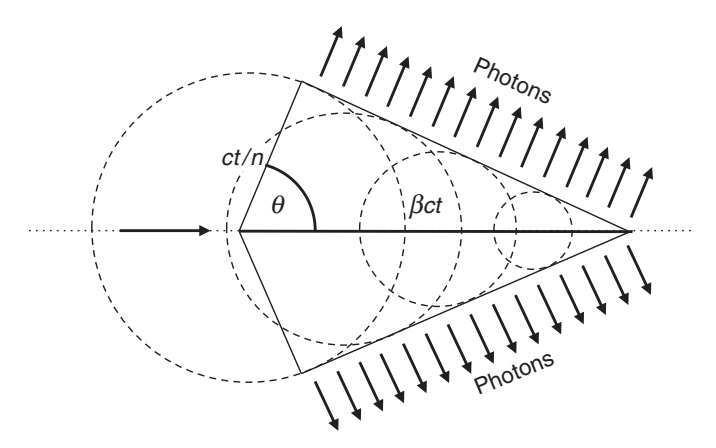
Organic scintillators are used extensively in modern particle physics experiments as a cost effective way to detect the passage of charged particles where precise spatial information is not required. In particular, detectors based on plastic and liquid scintillators have been used in a number of recent neutrino experiments. In an organic scintillator, the passage of a charged particle leaves some of the molecules in an excited state. In a scintillator, the subsequent decay of the excited state results in the emission of light in the ultraviolet (UV) region. By adding fluorescent dyes to the scintillator, the molecules of the dye absorb the UV light and re-emit it as photons in the blue region. The blue light can be detected by using photomultiplier devices which are capable of detecting single optical photons.

Čerenkov radiation

Charged particles can also be detected through their emission of Čerenkov radiation. When a charged particle traverses a dielectric medium of refractive index n it polarises the molecules in the medium. After its passage, the molecules return to the unpolarised state through the emission of photons. If the velocity of the particle is greater than the speed of light in that medium, v > c/n, constructive interference occurs and Čerenkov radiation is emitted as a coherent wavefront at a fixed angle θ to the trajectory of the charged particle, analogous to the sonic boom produced by supersonic aircraft. The angle at which the radiation is emitted is given by the geometrical construction shown in Figure 1.15. In a time t, the particle travels a distance θct . In this time the wavefront emitted at t = 0 has travelled a distance ct/n and therefore the angle θ at which the radiation is produced is given by

$$\cos\theta = \frac{1}{n\beta}.$$

The photons emitted as Čerenkov radiation can be detected using photo-multiplier tubes (PMTs), capable of detecting a single photon with reasonable efficiency. Čerenkov radiation can be used to detect relativistic particles in large volumes of transparent liquid (for example water) as has been used extensively in the detection



of neutrinos. Furthermore, Čerenkov radiation is emitted only when $\beta > 1/n$. This threshold behaviour can be utilised to aid the identification of particles of a given momentum p; for a relativistic particle $\beta = pc/E = p/(p^2 + m^2c^2)^{1/2}$ and therefore only particles with mass

$$mc < (n^2 - 1)^{1/2} p$$

will produce Čerenkov radiation.

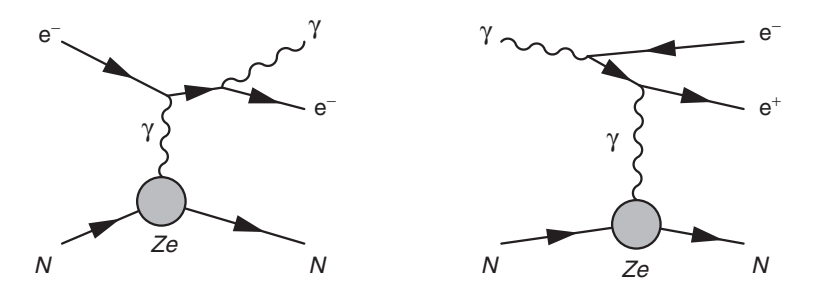
1.2.2 Interactions and detection of electrons and photons

At low energies, the energy loss of electrons is dominated by ionisation. However, for energies above a "critical energy" E_c , the main energy loss mechanism is bremsstrahlung (German for braking radiation), whereby the electron radiates a photon in the electrostatic field of a nucleus, as shown in Figure 1.16. The critical energy is related to the charge Z of the nucleus and is approximately

$$E_c \sim \frac{800}{Z} \, \text{MeV}.$$

The electrons of interest in most particle physics experiments are in the multi-GeV range, significantly above the critical energy, and therefore interact with matter primarily through bremsstrahlung. The bremsstrahlung process can occur for all charged particles, but the rate is inversely proportional to the square of the mass of the particle. Hence, for muons the rate of energy loss by bremsstrahlung is suppressed by $(m_e/m_\mu)^2$ relative to that for electrons. It is for this reason that bremsstrahlung is the dominant energy-loss process for electrons, but ionisation energy loss dominates for muons (except at very high energies, $E_\mu > 100\,\text{GeV}$, where bremsstrahlung also contributes).

At low energies, photons interact in matter primarily by the photoelectric effect, whereby the photon is absorbed by an atomic electron that is ejected from the atom. At somewhat higher energies, $E_{\gamma} \sim 1$ MeV, the Compton scattering process $\gamma e^- \rightarrow \gamma e^-$ becomes significant. At higher energies still, $E_{\gamma} > 10$ MeV, the interactions of photons are dominated by e^+e^- pair production in the field of the nucleus, as shown in Figure 1.16.



The bremsstrahlung and e^+e^- pair-production processes. N is a nucleus of charge +Ze.

The electromagnetic interactions of high energy electrons and photons in matter are characterised by the *radiation length* X_0 . The radiation length is the average distance over which the energy of an electron is reduced by bremsstrahlung by a factor of 1/e. It is also approximately 7/9 of the mean free path of the e^+e^- pair-production process for a high-energy photon. The radiation length is related to the atomic number Z of the material, and can be approximated by the expression

$$X_0 \approx \frac{1}{4\alpha n Z^2 r_{\rm e}^2 \ln{(287/Z^{1/2})}},$$

where n is the number density of nuclei and $r_{\rm e}$ is the "classical radius of the electron" defined as

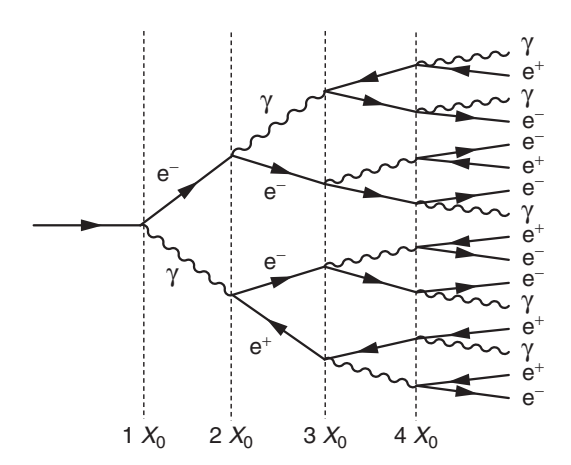
$$r_{\rm e} = \frac{e^2}{4\pi\epsilon_0 m_{\rm e}c^2} = 2.8 \times 10^{-15} \,\mathrm{m}.$$

For high-Z materials the radiation length is relatively short. For example, iron and lead have radiation lengths of $X_0(\text{Fe}) = 1.76 \text{ cm}$ and $X_0(\text{Pb}) = 0.56 \text{ cm}$.

Electromagnetic showers

When a high-energy electron interacts in a medium it radiates a bremsstrahlung photon, which in turn produces an e⁺e⁻ pair. The process of bremsstrahlung and pair production continues to produce a cascade of photons, electrons and positrons, referred to as an electromagnetic shower, as indicated in Figure 1.17. Similarly, the primary interaction of a high-energy photon will produce an e⁺e⁻ pair that will then produce an electromagnetic shower.

The number of particles in an electromagnetic shower approximately doubles after every radiation length of material traversed. Hence, in an electromagnetic



The development of an electromagnetic shower where the number of particles roughly doubles after each radiation length.

shower produced by an electron or photon of energy E, the average energy of the particles after x radiation lengths is

$$\langle E \rangle \approx \frac{E}{2^x}.$$
 (1.3)

The shower continues to develop until the average energy of the particles falls below the critical energy E_c , at which point the electrons and positrons in the cascade lose energy primarily by ionisation. The electromagnetic shower therefore has the maximum number of particles after x_{max} radiation lengths, given by the condition $\langle E \rangle \approx E_c$. From (1.3) it can be seen that this point is reached after

$$x_{max} = \frac{\ln (E/E_c)}{\ln 2}$$

radiation lengths. In a high-Z material, such as lead with $E_c \sim 10\,\mathrm{MeV}$, a 100 GeV electromagnetic shower reaches is maximum after $x_{max} \sim 13\,X_0$. This corresponds to less than 10 cm of lead. Consequently, electromagnetic showers deposit most of their energy in a relatively small region of space. The development of a shower is a stochastic process consisting of a number of discrete interactions. However, because of the large numbers of particles involved, which is of order $2^{x_{max}}$, the fluctuations in the development of different electromagnetic showers with the same energy are relatively small and individual electromagnetic showers of the same energy are very much alike.

Electromagnetic calorimeters

In high-energy particle physics experiments, the energies of electrons and photons are measured using an electromagnetic calorimeter constructed from high-Z materials. A number of different technologies can be used. For example, the electromagnetic calorimeter in the CMS detector at the LHC is constructed from an array of 75 000 crystals made from lead tungstate (PbWO₄), which is an inorganic scintillator. The crystals are both optically transparent and have a short radiation length $X_0 = 0.83$ cm, allowing the electromagnetic showers to be contained in a compact region. The electrons in the electromagnetic shower produce scintillation light that can be collected and amplified by efficient photon detectors. The amount of scintillation light produced is proportional to the total energy of the original electron/photon. Alternatively, electromagnetic calorimeters can be constructed from alternating layers of a high-Z material, such as lead, and an active layer in which the ionisation from the electrons in the electromagnetic shower can be measured. For the electromagnetic calorimeters in large particle physics detectors, the energy resolution for electrons and photons is typically in the range

$$\frac{\sigma_E}{E} \sim \frac{3\% - 10\%}{\sqrt{E/\text{GeV}}}.$$

1.2.3 Interactions and detection of hadrons

Charged hadrons (for example, protons and charged pions) lose energy continuously by the ionisation process as they traverse matter. In addition, both charged and neutral hadrons can undergo a strong interaction with a nucleus of the medium. The particles produced in this primary hadronic interaction will subsequently interact further downstream in the medium, giving rise to a cascade of particles. The development of hadronic showers is parameterised by the nuclear interaction interaction length λ_I defined as the mean distance between hadronic interactions of relativistic hadrons. The nuclear interaction length is significantly larger than the radiation length. For example, for iron $\lambda_I \approx 17$ cm, compared to its radiation length of 1.8 cm.

Unlike electromagnetic showers, which develop in a uniform manner, hadronic showers are inherently more variable because many different final states can be produced in high-energy hadronic interactions. Furthermore, any π^0 s produced in the hadronic shower decay essentially instantaneously by $\pi^0 \to \gamma\gamma$, leading to an electromagnetic component of the shower. The fraction of the energy in this electromagnetic component will depend on the number of π^0 s produced and will vary from shower to shower. In addition, not all of the energy in a hadronic shower is detectable; on average 30% of incident energy is effectively lost in the form of nuclear excitation and break-up.

Hadron calorimeters

In particle detector systems, the energies of hadronic showers are measured in a hadron calorimeter. Because of the relatively large distance between nuclear interactions, hadronic showers occupy a significant volume in any detector. For example, in a typical hadron calorimeter, the shower from a 100 GeV hadron has longitudinal and lateral extents of order 2 m and 0.5 m respectively. Therefore a hadron calorimeter necessarily occupies a large volume. A number of different technologies have been used to construct hadron calorimeters. A commonly used technique is to use a sandwich structure of thick layers of high-density absorber material (in which the shower develops) and thin layers of active material where the energy depositions from the charged particles in the shower are sampled. For example, the hadron calorimeter in the ATLAS experiment at the LHC consists of alternating layers of steel absorber and plastic scintillator tiles. The signals in the different layers of the scintillator tiles are summed to give a measure of the energy of the hadronic shower. Fluctuations in the electromagnetic fraction of the shower and the amount of energy lost in nuclear break-up limits the precision to which the energy can be measured to

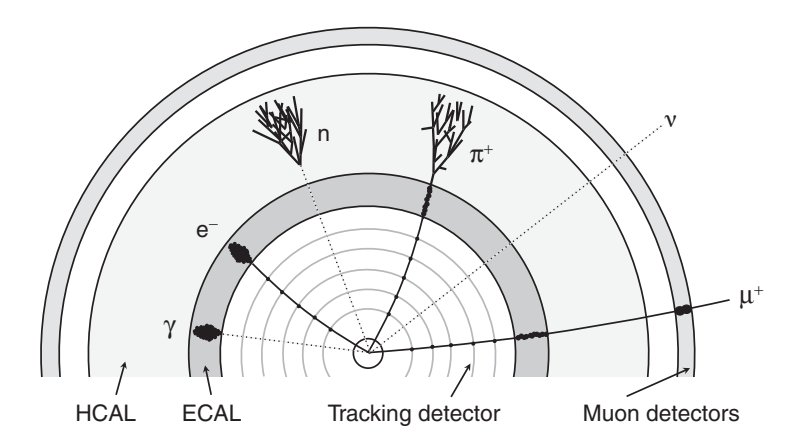
$$\frac{\sigma_E}{E} \gtrsim \frac{50\%}{\sqrt{E/\text{GeV}}},$$

which is roughly an order of magnitude worse than the energy resolution for electromagnetic showers.

1.3 Collider experiments

At a particle accelerator, the colliding beams produce individual interactions referred to as *events*. The large particle physics detector systems use a wide range of technologies to detect and measure the properties of the particles produced in these high-energy collisions with the aim of reconstructing the primary particles produced in the interaction. In essence, one tries to go from the signals in the different detector systems back to the Feynman diagram responsible for the interaction.

The basic structure of a modern particle physics detector is indicated in Figure 1.18. In general, a detector consists of a cylindrical (or polygonal) barrel part, with its axis parallel to the incoming colliding beams. The cylindrical structure is closed by two flat end caps, providing almost complete solid angle coverage down to the beam pipe. The inner region of the detector is devoted to the tracking of charged particles. The tracking volume is surrounded by an electromagnetic calorimeter (ECAL) for detecting electrons and photons. The relatively large-volume hadronic calorimeter (HCAL) for detecting and measuring the energies of hadrons is located outside the ECAL. Dedicated detectors are positioned at the outside of the experiment to record the signals from any high-energy muons produced in the collisions, which are the only particles (apart from neutrinos) that can penetrate through the HCAL. In order to be able to measure the momenta of



The typical layout of a large particle physics detector consisting of a tracking system (here shown with cylindrical layers of a silicon detector), an electromagnetic calorimeter (ECAL), a hadron calorimeter (HCAL) and muon detectors. The solenoid used to produce the magnetic field is not shown. The typical signatures produced by different particles are shown.

Fig. 1.18

charged particles, a detector usually has a solenoid which produces a strong axial magnetic field in the range B = 1-4 T. The solenoid may be located between the tracking volume and the calorimeters.

The design of a collider experiment is optimised for the identification and energy measurement of the particles produced in high-energy collisions. The momenta of charged particles are obtained from the curvature of the reconstructed tracks. The energies of neutral particles are obtained from the calorimeters. Particle identification is achieved by comparing the energy deposits in the different detector systems as indicated in Figure 1.18. Photons appear as isolated energy deposits in the ECAL. Electrons are identified as charged-particle tracks that are associated with an electromagnetic shower in the ECAL. Neutral hadrons will usually interact in the HCAL and charged hadrons are identified as charged-particle tracks associated with a small energy deposit in the ECAL (from ionisation energy loss) and a large energy deposition in the HCAL. Finally, muons can be identified as charged-particle tracks associated with small energy depositions in both the ECAL and HCAL and signals in the muon detectors on the outside of the detector system.

Whilst neutrinos leave no signals in the detector, their presence often can be inferred from the presence of *missing momentum*, which is defined as

$$\mathbf{p}_{mis} = -\sum_{i} \mathbf{p}_{i},$$

where the sum extends over the measured momenta of all the observed particles in an event. If all the particles produced in the collision have been detected, this sum should be zero (assuming the collision occurs in the centre-of-mass frame). Significant missing momentum is therefore indicative of the presence of an undetected neutrino.

The ultimate aim in collider experiments is to reconstruct the fundamental particles produced in the interaction. Electrons, photons and muons give clear signatures and are easily identified. Tau-leptons, which decay in 2.9×10^{-13} s, have to be identified from their observed decay products. The main tau-lepton decay modes are $\tau^- \to e^- \bar{\nu}_e \nu_\tau$ (17.8%), $\tau^- \to \mu^- \bar{\nu}_\mu \nu_\tau$ (17.4%), $\tau^- \to \pi^- (n\pi^0) \nu_\tau$ (48%) and $\tau^- \to \pi^- \pi^+ \pi^- (n\pi^0) \nu_\tau$ (15%). The hadronic decay modes typically lead to final states with one or three charged pions and zero, one or two π^0 s which decay to photons $\pi^0 \to \gamma \gamma$. Tau-leptons can therefore be identified as narrowly collimated jets of just a few particles and the presence of missing momentum in the event, associated with the neutrino.

1.3.1 Detection of quarks

Owing to the nature of QCD, quarks are never observed as free particles, but are always found confined within hadrons. However, in high-energy collisions it is

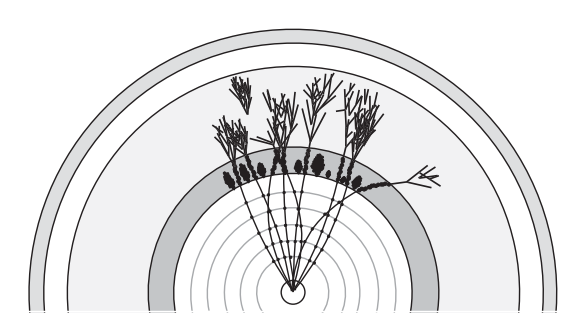


Fig. 1.19 An illustration of the appearance of a jet in a detector. In practice, the individual particles are not resolved.

quarks that are produced, not hadrons. For example, in the process $e^+e^- \to q\overline{q}$ the two quarks will be produced flying apart at relativistic velocities. As a result of the QCD interaction, the energy in the strong interaction field between the two quarks is converted into further pairs of quarks and antiquarks through a process call hadronisation (described in Chapter 10) that occurs over a distance scale of 10^{-15} m. As a result of hadronisation, each quark produced in a collision produces a jet of hadrons, as indicated in Figure 1.19. Hence a quark is observed as an energetic jet of particles. On average, approximately 60% of the energy in a jet is in the form of charged particles (mostly π^\pm), 30% of the energy is in the form of photons from $\pi^0 \to \gamma \gamma$ decays, and 10% is in the form of neutral hadrons (mostly neutrons and K_L s). In high-energy jets, the separation between the individual particles is typically smaller than the segmentation of the calorimeters and not all of the particles in the jet can be resolved. Nevertheless, the energy and momentum of the jet can be determined from the total energy deposited in the calorimeters.

Tagging of b-quarks

In general, it is not possible to tell which flavour of quark was produced, or even whether the jet originated from a quark or a gluon. However, if a b-quark is produced, the hadronisation process will create a jet of hadrons, one of which will contain the b-quark, for example a $\overline{B}^0(b\overline{d})$ meson. It turns out that b-quark hadrons are relatively long-lived with lifetimes of order 1.5×10^{-12} s. When produced in high-energy collisions, this relatively long lifetime, combined with the Lorentz time-dilation factor, means that B hadrons travel on average a few millimetres before decaying. The decays of B hadrons often produce more than one charged particle. Because of the relatively large mass of the b-quark, the decay products can be produced at a relatively large angle to the original b-quark direction. Therefore the experimental signature for a b-quark is a jet of particles emerging from the point of the collision (the primary vertex) and a secondary vertex from the b-quark decay,

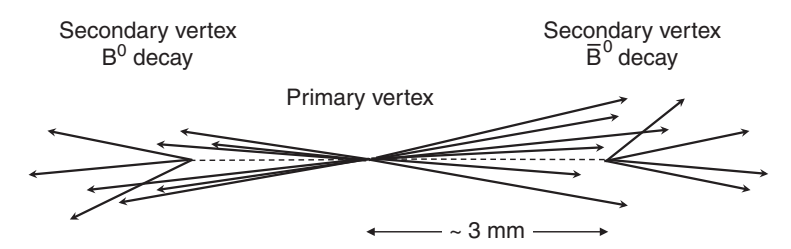


Fig. 1.20 An illustration of the principle of b-quark tagging in a $e^+e^- \rightarrow Z \rightarrow b\bar{b}$ event.

which is displaced from the primary vertex by several millimetres, as indicated in Figure 1.20.

The identification of b-quark jets relies on the ability to resolve the secondary vertices from the primary vertex. In practice, this is achieved by using high-precision silicon microvertex detectors consisting of several concentric layers of silicon at radii of a few centimetres from the axis of the colliding beams. Such detectors can achieve a single hit resolution of $O(10\,\mu\text{m})$, sufficient to be able to identify and reconstruct the secondary vertices, even in a dense jet environment. The ability to tag b-quarks has played an important role in a number of recent experiments.

1.4 Measurements at particle accelerators

With the exception of the measurements of the properties of the neutrino, most of the recent breakthroughs in particle physics have come from experiments at high-energy particle accelerators. Particle accelerators can be divided into two types: (i) colliding beam machines where two beams of accelerated particles are brought into collision; and (ii) fixed-target experiments where a single beam is fired at a stationary target. In order to produce massive particles, such as the W^{\pm} , Z and H bosons, high energies are required. More precisely, the energy available in the centre-of-mass frame has to be greater than the sum of the masses of the particles being produced. The centre-of-mass energy \sqrt{s} is given by the square root of the Lorentz invariant quantity s formed from the total energy and momentum of the two initial-state particles, which in natural units with c = 1 is

$$s = \left(\sum_{i=1}^{2} E_i\right)^2 - \left(\sum_{i=1}^{2} \mathbf{p}_i\right)^2.$$

In a fixed-target experiment, momentum conservation implies that the final-state particles are always produced with significant kinetic energy and much of the initial

Table 1.4	The basic parameters of the recent particle accelerators. At the time of writing the LHC was operating at $\sqrt{s}=8$ TeV.						
Collider	Laboratory	Type	Date	\sqrt{s}/GeV	Luminosity/cm ⁻² s ⁻¹		
PEP-II	SLAC	e+e-	1999–2008	10.5	1.2×10^{34}		
KEKB	KEK	e^+e^-	1999–2010	10.6	2.1×10^{34}		
LEP	CERN	e^+e^-	1989-2000	90-209	10^{32}		
HERA	DESY	e^-p/e^+p	1992-2007	320	8×10^{31}		
Tevatron	Fermilab	p p	1987-2012	1960	4×10^{32}		
LHC	CERN	pp	2009–	14 000	10^{34}		

energy is effectively wasted. For example, if an E = 7 TeV proton collides with a proton at rest,

$$s = (E + m_{\rm p})^2 - p^2 = 2m_{\rm p}^2 + 2m_{\rm p}E \approx 2m_{\rm p}E,$$

giving a centre-of-mass energy of just 115 GeV. Colliding beam machines have the advantage that they can achieve much higher centre-of-mass energies since the collision occurs in the centre-of-mass frame. For example, the LHC will ultimately collide two beams of 7 TeV protons giving a centre-of-mass energy of 14 TeV. For this reason, almost all high-energy particle physics experiments are based on large particle colliders.

Only charged stable particles can be accelerated to high energies, and therefore the possible types of accelerator are restricted to e^+e^- colliders, hadron colliders (pp or $p\bar{p}$) and electron–proton colliders (e^-p or e^+p). The most recent examples have been the Tevatron $p\bar{p}$ collider, the LHC pp collider, the LEP e^+e^- collider, the PEP-II and KEKB e^+e^- b-factories, and the HERA electron–proton collider. The main parameters of these machines are summarised in Table 1.4. The two most important features of an accelerator are its centre-of-mass energy, which determines the types of particles that can be studied/discovered, and its instantaneous luminosity \mathcal{L} , which determines the event rates. For a given process, the number of interactions is the product of the luminosity integrated over the lifetime of the operation of the machine and the *cross section* for the process in question,

$$N = \sigma \int \mathcal{L}(t) \, \mathrm{d}t. \tag{1.4}$$

The cross section (defined in Chapter 3) is a measure of quantum mechanical probability for the interaction. It depends on the fundamental physics involved in the Feynman diagram(s) contributing to the process.

In order to convert the observed numbers of events of a particular type to the cross section for the process, the integrated luminosity needs to be known. In principle, this can be calculated from the knowledge of the parameters of the colliding beams. Typically, the particles in an accelerator are grouped into bunches that are

27 Summary

brought into collision at one or more interaction points where the detectors are located. In the case of the LHC, the bunches are separated by 25 ns, corresponding to a collision frequency of $f = 40 \,\mathrm{MHz}$. The instantaneous luminosity of the machine can be expressed in terms of the numbers of particles in the colliding bunches, n_1 and n_2 , the frequency at which the bunches collide, and the root-mean-square (rms) horizontal and vertical beam sizes σ_x and σ_y . Assuming that the beams have a Gaussian profile and collide head-on, the instantaneous luminosity is given by

$$\mathcal{L} = f \frac{n_1 n_2}{4\pi \,\sigma_x \sigma_u}.\tag{1.5}$$

In practice, the exact properties of the colliding beams, such as the transverse profiles, are not known precisely and it is not possible to accurately calculate the instantaneous luminosity. For this reason, cross section measurements are almost always made with reference to a process where the cross section is already known. Hence, a cross section measurement is performed by counting the number of events of interest N, and the number of observed events for the reference process N_{ref} , such that the measured cross section is given by

$$\sigma = \sigma_{\rm ref} \frac{N}{N_{\rm ref}}.$$

Corrections may needed to account for the detection efficiency and possible sources of background events. Nevertheless, ultimately many experimental particle physics measurements reduce to counting events, where the event type is identified using the experimental techniques described in Section 1.3. Of course, this is not always quite as easy as it sounds.

Summary

The intention of this chapter was to introduce some of the basic ideas of particle physics. At this point you should be familiar with the types of particles and forces in the Standard Model and you should have a qualitative understanding of how to use the Standard Model vertices associated with the electromagnetic, strong and weak interactions to construct Feynman diagrams for particle interactions and decays. The second part of the chapter introduced the experimental techniques of particle physics and is intended to provide the context for the experimental measurements used to demonstrate the theoretical ideas developed in the following chapters. At this point you should understand how the different particles appear in the large detector systems employed in collider experiments.